Concerted two-proton-coupled electron transfer from piceatannol to electrogenerated superoxide in *N*,*N*-dimethylformamide

*Tatsushi Nakayama**,† and *Bunji Uno*†,‡,[1]

†Department of Pharmacy, Gifu Pharmaceutical University, 1-25-4 Daigaku-nishi, Gifu 501-1196, Japan

‡United Graduate School of Drug Discovery and Medical Information Sciences, Gifu University, 1-1 Yanagido, Gifu 501-1193, Japan

*Phone: +81-58-230-8100 Fax: +81-58-230-8200 E-mail: tnakayama@gifu-pu.ac.jp

KEYWORDS

Electrochemistry; density functional theory; piceatannol; superoxide; two-proton-coupled electron transfer

1

[1] Current address: Faculty of Pharmacy, Gifu University of Medical Science, 4-3-3 Nijigaoka, Kani, Gifu 509-0923, Japan

ABSTRACT

The reactivity of 4-[(*E*)-2-(3,5-dihydroxyphenyl)ethenyl]benzene-1,2-diol (piceatannol) toward electrochemically generated superoxide radical anion ($O_2^{\bullet-}$) was investigated using electrochemistry and in situ controlled-potential electrolytic electron spin resonance (ESR) measurements in *N*,*N*-dimethylformamide with density functional theory (DFT) calculations. The quasireversible cyclic voltammogram of dioxygen/$O_2^{\bullet-}$, modified in the presence of piceatannol, indicated that the electrogenerated $O_2^{\bullet-}$ was scavenged by piceatannol via proton-coupled electron transfer. Differences in the reactivities of piceatannol and 5-[(*E*)-2-(4-hydroxyphenyl)ethen-1-yl]benzene-1,3-diol (*trans*-resveratrol) toward $O_2^{\bullet-}$, originating from the presence of the benzene-1,2-diol (catechol) moiety, were observed in the voltammograms and ESR measurements. The electrochemical and computational results show that the reaction mechanism is a concerted two-proton-coupled electron transfer (2PCET) via the catechol moiety of piceatannol. The stilbene moiety of piceatannol kinetically promotes 2PCET via its catechol moiety. These findings indicate that piceatannol is a better $O_2^{\bullet-}$ scavenger than catechol and *trans*-resveratrol.

1. INTRODUCTION

4-[(*E*)-2-(3,5-Dihydroxyphenyl)ethen-1-yl]benzene-1,2-diol (piceatannol, $PiceH_4$) is a type of phenolic antioxidant, a stilbenoid,[1] and a phytoalexin,[2] found in mycorrhizal and nonmycorrhizal roots of Norway spruces,[3] the seeds of the palm Aiphanes horrida[4] and Gnetum cleistostachyum.[5] Piceatannol is an analog and also a metabolite of 5-[(*E*)-2-(4-Hydroxyphenyl)ethen-1-yl]benzene-1,3-diol (*trans*-resveratrol, $RsvH_3$). In vitro studies have shown that piceatannol exhibits pharmacological effects against leukemia and non-Hodgkin's lymphoma, making it

valuable as a multitarget molecule against various diseases.[6] In particular, piceatannol can scavenge the reactive oxygen species (ROS), potentially playing a therapeutic role as an antioxidant.[7,8] However, mechanistic insights into the therapeutic effects of piceatannol are yet to be demonstrated.

Chemical reactions including electron transfer (ET) to scavenge ROS such as superoxide radical anion ($O_2^{\bullet-}$), hydroperoxyl radical ($HO_2^{\bullet}$), and hydroxyl radical ($HO^{\bullet}$), must be demonstrated to confirm the medicinal effects of piceatannol. Clarifying the ROS scavenging mechanism of piceatannol is a prerequisite to elucidate its medicinal effects, as ROS generated around lesions and inflammatory organs may directly cause several pathologies[7,8] Cordova-Gomez et al. investigated the peroxyl radical scavenging activity of piceatannol using density functional theory (DFT), compared it with that of *trans*-resveratrol—its structural analog,[9] and concluded that piceatannol is a better peroxyl scavenger than *trans*-resveratrol. Piceatannol belongs to the stilbenoid group of polyphenols and possesses a benzene-1,2-diol (ortho-diphenol, catechol) moiety and another phenolic ring linked to each other by an ethylene bridge with four hydroxyl groups (OH). Effective antioxidant activity is related to the quinone–hydroquinone π-conjugation characterized by the presence of ortho- or para-diphenolic OHs. The better ROS scavenging of piceatannol compared with that of *trans*-resveratrol[10] is potentially due to the functionality of its catechol moiety, which can delocalize π-electrons with its resonance structure. However, the reactions of isolated $HO_2^{\bullet}$ and $HO^{\bullet}$ are difficult to observe experimentally; because they are highly reactive. Consequently, deeper insights into the ROS scavenging mechanism of piceatannol remain unclear.

The antioxidant activities of polyphenol stilbenoids have been extensively studied using different assays and methodologies regarding the structure–activity or structure–property

relationship related to the position and number of OHs,[10–14] and the electron-donating ability of stilbenoids has been discussed. Further, experimental data demonstrate that if the OH is scavenged or replaced by the methoxy group, the molecule loses its activity, suggesting that the OH is a proton donor and substituent with an electronic inductive effect.[14] Thus, ROS scavenging activity was evaluated using the bond dissociation energy and ionization potential of the OH representing the antioxidant property of the individual OHs and entire molecule of stilbenoids. Consequently, several ROS scavenging mechanisms exist for piceatannol and other phenolic antioxidants, such as superoxide-facilitated oxidation,[15–17] single-electron transfer (SET), sequential proton-loss ET,[18] hydrogen-atom transfer (HAT), and proton-coupled electron transfer (PCET).[19–23] At present, the antioxidant mechanism involves ET and proton transfer (PT); thus, HAT involving PCET via hydrogen bonds (HBs) is a plausible ROS scavenging/antioxidant mechanism rather than SET.

We previously analyzed the PCET reaction between electrogenerated $O_2^{\bullet-}$ and phenolic antioxidants, 1,2- and 1,4-benzendiols,[24,25] 1,2- and 1,4-dihydroxynaphthalenes,[26] and monophenols including tocopherols and aminophenols,[27,28] polyphenols, and *trans*-resveratrol,[29] in *N*,*N*-dimethylformamide (DMF). Here, $O_2^{\bullet-}$ cannot accept electrons from phenolic substrates because $O_2^{\bullet-}$ is not so electrophilic; however, $HO_2^{\bullet}$ (a protonated form of $O_2^{\bullet-}$) is a strong oxidant. Thus, ET and PT from antioxidants/deprotonated anion to $O_2^{\bullet-}$/$HO_2^{\bullet}$ are closely related, potentially embodying the actual scavenging mechanism. Among them, concerted two-proton-coupled electron transfer (2PCET)—a type of PCET mechanism characterized by quinone–hydroquinone π-conjugation via the catechol moiety—is necessary for the efficient scavenging of $O_2^{\bullet-}$.[23–26] Conversely, *trans*-resveratrol scavenges $O_2^{\bullet-}$ through a PT forming $HO_2^{\bullet}$ followed by a concerted PCET via 4′OH, where the stilbene moiety is essential for the PCET.[29] Notably,

piceatannol possesses catechol and stilbene moieties, although it remains unclear how they contribute to $O_2^{\bullet-}$ scavenging via PCET.[9–11,13,30–32]

Herein, we investigated the reaction mechanism between piceatannol and electrogenerated $O_2^{\bullet-}$ in DMF by focusing on the role of the catechol and stilbene moieties of piceatannol. Next, we clarified which moiety primarily plays a functional role in the $O_2^{\bullet-}$ scavenging, showing the differences between piceatannol and *trans*-resveratrol. Accordingly, we reveal the $O_2^{\bullet-}$ scavenging mechanism of piceatannol, which is important for understanding its health benefits to use.

Chart 1. Structures of the compounds considered in this study

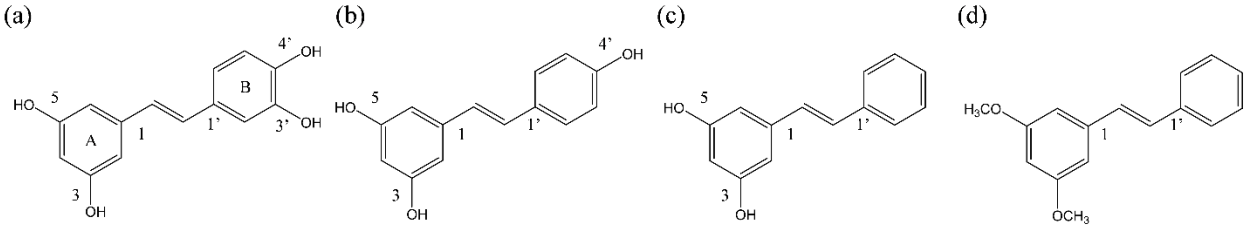

(a) 4-[(*E*)-2-(3,5-Dihydroxyphenyl)ethen-1-yl]benzene-1,2-diol (piceatannol), (b) 5-[(*E*)-2-(4-hydroxyphenyl)ethen-1-yl]benzene-1,3-diol (*trans*-resveratrol), (c) 5-[(1*E*)-2-phenylethen-1-yl]benzene-1,3-diol (pinosylvin), and (d) 1,3-dimethoxy-5-[(*E*)-2-phenylethenyl]benzene (3,5-dimethoxystilbene)

2. MATERIALS AND METHODS

2.1. Chemicals

Piceatannol (>98.0%), *trans*-resveratrol (>99.0%), 5-[(1*E*)-2-phenylethen-1-yl]benzene-1,3-diol (pinosylvin, >97.0%), 1,3-dimethoxy-5-[(*E*)-2-phenylethenyl]benzene (3,5-dimethoxystilbene, >98.0%), and anhydrous DMF (>99.9%) for electrochemical and electrolytic electron spin resonance (ESR) spectral measurements purchased from Sigma-Aldrich Inc.

(Tokyo, Japan) were used as received. We purchased tetrapropylammonium perchlorate (TPAP, >98.0%) from Tokyo Chemical Industry Co., Ltd. (Tokyo, Japan) and prepared for a supporting electrolyte as described previously.[33] Dinitrogen (N_2, 99.0%) and O_2 (99.0%) gasses were purchased from Medical Sakai Co., Ltd. (Gifu, Japan). Ferrocene (Fc)—used as a reference for the electrochemical potential—was purchased from Nacalai Tesque Inc. (Kyoto, Japan) and used as received.

2.2. Electrochemistry and in situ controlled-potential electrolytic ESR spectral measurements

Electrochemical measurement was conducted in a three-electrode system comprising working electrode: a 1.0-mm-diameter glassy carbon (GC), counter electrode: a coiled platinum (Pt, 99.99%), and reference electrode: a silver/silver nitrate ($Ag/AgNO_3$) containing tetrabutylammonium perchlorate (0.1 mol dm^{-3}) in an acetonitrile solution and $AgNO_3$ (0.01 mol dm^{-3}). A ferrocenium ion/ferrocene couple (Fc^+/Fc) was used for calibration of the reference electrode. The working electrode was polished with alumina paste, rinsed with deionized water and acetone, and air-dried before the experiments. Data collection was conducted using an ECstat-301 electrochemical analyzer (EC-frontier Co., Ltd., Kyoto, Japan) at 25°C (Supporting Information, Table S1). ESR spectra were obtained using a JES-X320 X-band spectrometer (JEOL Ltd., Tokyo, Japan). Controlled-potential electrolysis was performed in an ESR cell with a Pt working electrode (straight Pt wire with 0.5-mm-diameter sealed in a glass capillary) at 20°C (Supporting Information, Figure S1). Samples were prepared in a glovebox filled with dried N_2 gas to prevent moisture contamination of samples. Weakly basic DMF was used as the solvent for the aprotic electrochemistry of $O_2/O_2^{\bullet-}$ to avoid free proton-derived electrode noise. DMF solutions containing TPAP (0.1 mol dm^{-3}) were saturated with O_2 by air-bubbling the gas

112 for ca. 2–3 min. During the electrochemical and spectroelectrochemical measurements, O_2 gas
113 was passed over the solutions for keeping a constant concentration (4.8×10^{-3} mol dm^{-3}).

114 3. Theory and calculation

115 Solution-phase DFT calculations were conducted using three hybrid functionals: the Becke
116 three-parameter Lee–Yang–Parr functional (B3LYP), the meta exchange-correlated functional
117 (M06-2X),[34] and TPSSh,[35,36] implemented in the Gaussian 16 Program package.[37] We chose
118 these functionals because they provide good geometries of the reactants, products, and transition
119 states (TS) in PCET reactions. The energies of the highest occupied molecular orbital (HOMO)
120 and the lowest unoccupied molecular orbital (LUMO) were obtained from optimized geometry
121 based on frontier orbital theory. The standard split-valence triple ζ basis sets augmented by the
122 polarization d,p and diffusion orbitals 6-311+G(d,p) were applied in the calculations. The
123 polarized continuum model (PCM) was employed for the solvent contribution to the standard
124 Gibbs free energies under the default settings of Gaussian 16. The standard Gibbs energies at
125 298.15 K were obtained from internal energies using thermal correction, zero-point energies, and
126 entropy. Population analysis using the natural bond orbital (NBO) technique was performed to
127 obtain the numbers of electrons and spins.[38]

128 4. RESULT AND DISCUSSION

129 4.1. Cyclic voltammetry analyses of $O_2/O_2^{\bullet-}$ in the presence of piceatannol

130 Cyclic voltammograms (CVs) of O_2 (4.8×10^{-3} mol dm^{-3}) with $PiceH_4$ (a), $RsvH_3$ (b),
131 pinosylvin (c), and 3,5-dimethoxystilbene (d) were measured in DMF (Figure 1). The CVs
132 shown in Figures 1(b) and 1(c)[29] are for comparison. In the CVs, O_2 is reduced by one electron
133 generating $O_2^{\bullet-}$ in the cathodic scan, and reoxidized to O_2 in the anodic scan (Equation (1)),
134 where CV demonstrates a quasireversible redox couple of $O_2/O_2^{\bullet-}$ with cathodic/anodic peaks

(pc1/pa1, bold lines in Figure 1). The quasireversible CVs of $O_2/O_2^{\bullet-}$ (Equation (1)) show no change in (d) but became irreversible in the presence of the phenolic stilbenoids as proton donors (a)–(c) at 0–5.0 × 10^{-3} mol dm^{-3} concentrations, where CVs of the stilbenoids (Charts 1(a)–1(d)) without O_2 under bubbling N_2 gas demonstrated no peaks over the potential range (Figure 1(a)) (dotted black line, data not shown for Figures 1(b)–1(d)). Thus, the loss of reversibility of the CVs ($O_2/O_2^{\bullet-}$) was caused by an acid–base reaction, where $O_2^{\bullet-}$ (a Brønsted base) forms $HO_2^{\bullet}$ along the initial PT from the OH of acidic stilbenoids (Equation (2)).

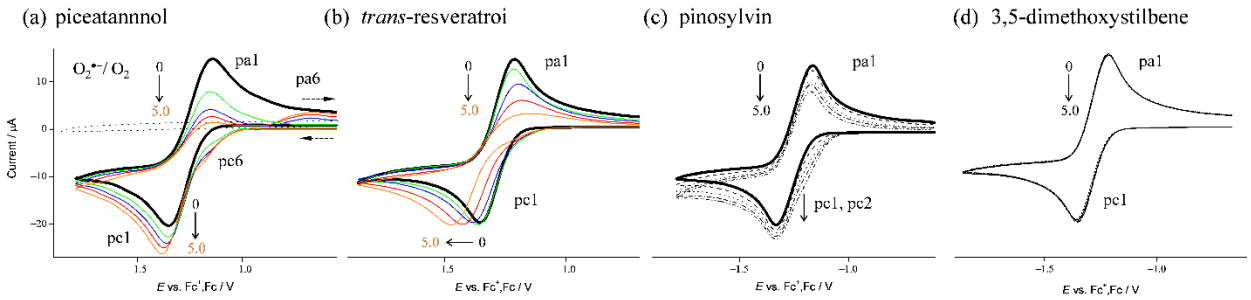

Figure 1. CVs of O_2 (4.8 × 10^{-3} mol dm^{-3}) with (a) piceatannol, (b) *trans*-resveratrol, (c) pinosylvin, and (d) 3,5-dimethyxystilbene in DMF containing TPAP (0.1 mol dm^{-3}); CV of (a) piceatannol without O_2 is shown as a control (dotted black line). CVs were recorded using a GC working electrode at 0.1 V s^{-1}. Concentrations are (a, b) 0 (black), 1.0 (green), 2.0 (blue), 3.0 (red), and 5.0 (orange), and (c, d) 0, 1.0, 3.0, and 5.0 (×10^{-3} mol dm^{-3}, the concentration of stilbenoids are shown by arrows).

Based on the loss of reversibility, the reactivity of piceatannol ($PiceH_4$) toward $O_2^{\bullet-}$ was greater than those of *trans*-resveratrol ($RsvH_3$) and pinosylvin. A prepeak (pc6 on pc1) and pa6 appear in Figure 1(a) in the presence of $PiceH_4$, which is different from those obtained with $RsvH_3$ (b). In addition, the appearance of the anodic peak with $PiceH_4$ differs from the overall reduction of O_2 to H_2O_2 observed with pinosylvin (Figure 1(c), cathodic peak: pc2 on pc1),

154 which involves the generation and subsequent heterogeneous reduction of $HO_2^{\bullet}$ (Equation (3))
155 showing a bielectronic CV.

156 $O_2 + e^- \leftrightarrow O_2^{\bullet-}$ $E°_{Ox,Red} = -1.284$ V vs. Fc^+/Fc (1)

157 $PiceH_4 + O_2^{\bullet-} \rightarrow PiceH_3^- + HO_2^{\bullet}$ the initial PT (2)

158 $HO_2^{\bullet} + e^- \rightarrow HO_2^-$ $E°_{Ox,Red} = -0.4$ to -0.2 V vs. Fc^+/Fc (3)

159 Next, two CVs demonstrating the $O_2^{\bullet-}/HO_2^{\bullet}$ scavenging by $PiceH_4$ and $RsvH_3$ (Figures 1(a)
160 and 1(b)) are compared. The cathodic curve with $RsvH_3$ (Figure 1(b)) considerably shifts to the
161 negative-potential side (where its cathodic peak potential shifted from −1.355 to −1.474 V vs
162 Fc^+/Fc), depending on the concentration of $RsvH_3$ (0–5.0×10^{-3} mol dm^{-3}). Conversely, the CV
163 with $PiceH_4$ (Figure 1(a)) showed no shift. This difference in the cathodic curves was due to the
164 difference in the PCET mechanism, originating from the structures of $PiceH_4$ and $RsvH_3$. The
165 shift in the presence of $RsvH_3$ is characteristic of the PCET among an extensive HB network
166 formed between multiple OHs involving meta OH (3OH/5OH) on the stilbene moiety and
167 $O_2/O_2^{\bullet-}$.[29] Therefore, the difference in the cathodic curve of $PiceH_4$ from that of $RsvH_3$ was
168 possibly due to the 3′OH of $PiceH_4$, which comprised the catechol moiety reacting preferentially
169 over the formation of HBs with 3OH/5OH.

170 To analyze the electrochemical mechanism shown in the CVs with $PiceH_4$ (Figure 1(a)), we
171 further measured three types of CVs for the same solution containing O_2 and $PiceH_4$ using (a) a
172 1.0 V s^{-1} scan rate, (b) two cycles of continuous scanning, and (c) two cycles of continuous
173 scanning at various scan rates (0.5–4.0 V s^{-1}) with the results divided by the square roots of the
174 scan rates (Figure 2).

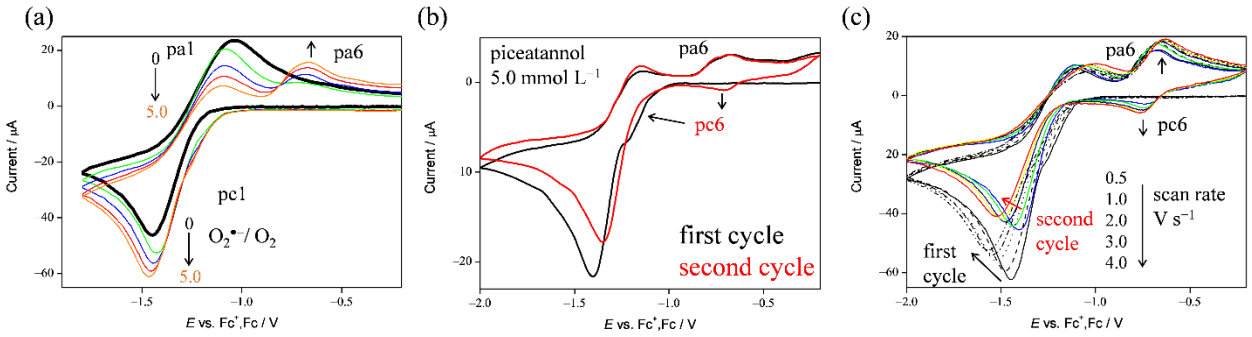

Figure 2. CVs of O_2 (4.8×10^{-3} mol dm^{-3}) with piceatannol in DMF containing TPAP (0.1 mol dm^{-3}), (a) at 1.0 V s^{-1} with piceatannol concentrations of 0 (black), 1.0 (green), 2.0 (blue), 3.0 (red), and 5.0 (orange) $\times$ 10^{-3} mol dm^{-3} (b) the first (black) and second (red) cycles of continuous scanning at 0.1 V s^{-1} with 5.0×10^{-3} mol dm^{-3} piceatannol concentration, and (c) two cycles of CVs (the first cycle: black, and the second cycle: colored) at various scan rates (0.5, 1.0, 2.0, 3.0, and 4.0 V s^{-1}, respectively) with 5.0×10^{-3} mol dm^{-3} piceatannol concentration. CVs were recorded using a GC working electrode, and the concentrations (a) and scan rates (c) are indicated by arrows.

Figure 2(a) shows CVs at 1.0 V s^{-1} (scan rate) similar to those in Figure 1(a) (0.1 V s^{-1}), demonstrating a quasireversible redox couple of $O_2/O_2^{\bullet-}$ and the loss of reversibility with $PiceH_4$. The slight difference is that pa6 is clearer and larger in Figure 2(a) than in Figure 1(a). Next, in the cathodic scan of the second cycle (red line) in Figure 2(b), a peak is observed at the position corresponding to the redox couple with pa6, and the prepeak observed in the cathodic scan of the first cycle (pc6 on pc1) disappears. The potential of pa6 differed between the first and second cycles, indicating that pa6 was derived from the product of a series of PCET reactions triggered by the electrogeneration of $O_2^{\bullet-}$, i.e., the pc6/pa6 peaks plausibly originated from a reversible redox of a product of the PCET from $PiceH_4$ to $O_2^{\bullet-}$. The PCET involves the initial PT (Equation (2)) followed by ET (Equation (4)) from the deprotonated anion ($PiceH_3^-$) to $HO_2^{\bullet}$, forming a

substrate radical ($PiceH_3^{\bullet}$) and a hydroperoxyl anion (HO_2^-). In addition, Figure 2(c) demonstrates the effects of scan rates on the second cycle of CV. As the scan rate increases, the bielectronic cathodic peak (pc6 on pc1 in the both of first and second cycles) becomes smaller, because the slow diffusion of substances in the electrode surface usually limits the electrode process. Nevertheless, the pc6/pa6 couple in the second cycle becomes larger. These CV appearances with scan rate dependency demonstrated that the reversible redox (pc6/pa6) appeared in the second cycle scan that derived from a quinoid radical as a product of the PCET. We speculated that a quinoid radical derived from the catechol moiety at the B ring of $PiceH_4$ was formed after the second PT (Equation (5)) for its chemical reversibility. Conversely, the bielectronic CV behavior was not observed in the presence of $RsvH_3$ (Figure 1(b)) owing to the ET scavenging $HO_2^{\bullet}$ and subsequent degradation of the generated radical.

$$HO_2^{\bullet} + PiceH_3^- \rightarrow HO_2^- + PiceH_3^{\bullet} \qquad \text{ET} \qquad (4)$$

$$HO_2^- + PiceH_3^{\bullet} \rightarrow H_2O_2 + PiceH_2^{\bullet-} \qquad \text{the second PT} \qquad (5)$$

Based on the CV results, the electrochemical mechanisms of $O_2/O_2^{\bullet-}$ with acidic stilbenoids (Figures 1(a)–1(c)) are plausibly summarized in Figure 3, including Equations (1)–(5). The CV results recorded with $PiceH_4$ and $RsvH_3$ (Figures 1(a) and 1(b)) demonstrated the scavenging of $O_2^{\bullet-}/HO_2^{\bullet}$ via PCET (Figure 3(a)), involving Equations (1), (2), (4), and (5). Conversely, the CV result with pinosylvin (Figure 1(c)) demonstrated the absence of $O_2^{\bullet-}/HO_2^{\bullet}$ scavenging (Figure 3(b)), showing the electro–chemical–electro processes of O_2/HO_2^- (Equations (1)–(3)). Thus, the comparison revealed that the B ring (the mono phenolic moiety of $RsvH_3$ and the catechol moiety of $PiceH_4$) provided mechanistic insights into the $O_2^{\bullet-}/HO_2^{\bullet}$ scavenging via the PCET mechanism.

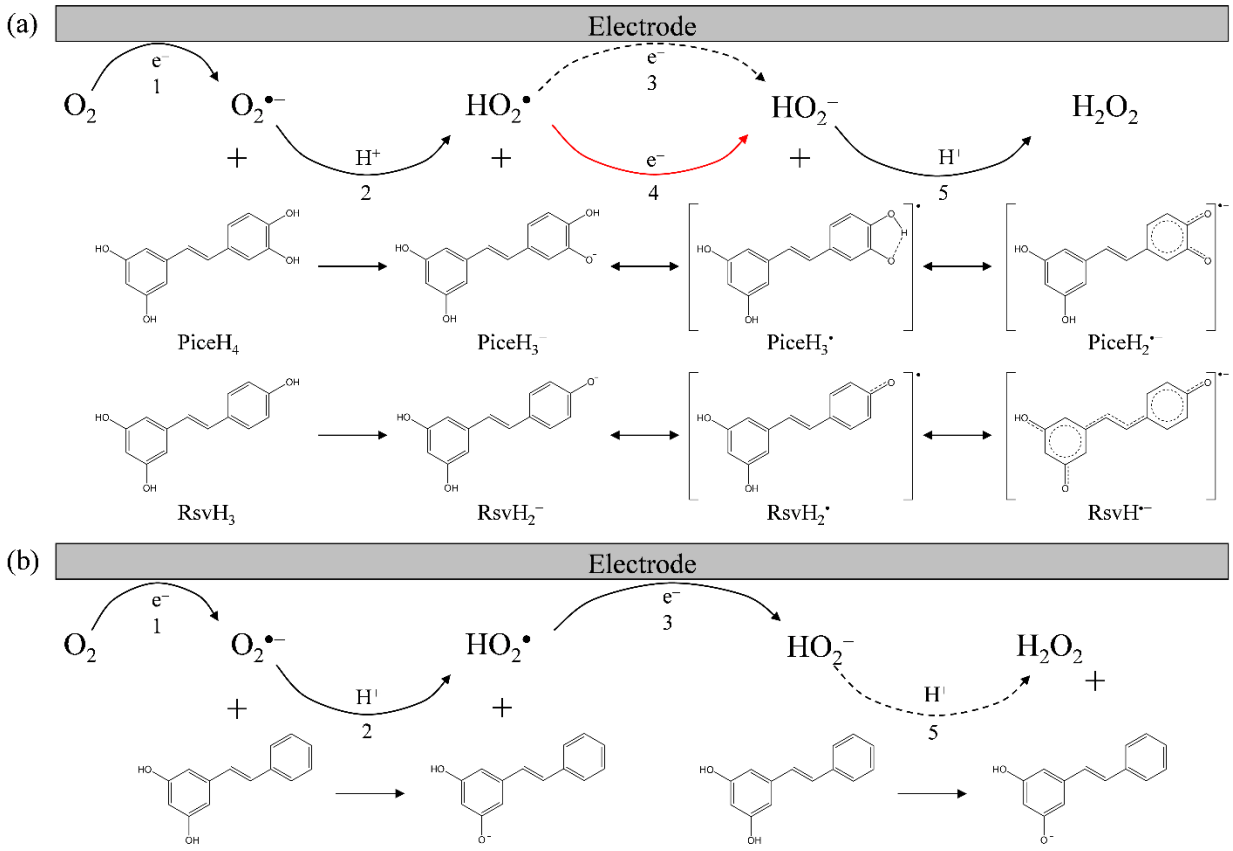

Figure 3. Electrochemical mechanisms of $O_2/O_2^{\bullet-}$ with (a) piceatannol ($PiceH_4$), *trans*-resveratrol ($RsvH_3$), and (b) pinosylvin in DMF; [1]one-electron reduction of $O_2/O_2^{\bullet-}$, [2]proton transfer from the acidic stilbenoid to $O_2^{\bullet-}$, [3]one-electron reduction of $HO_2^{\bullet}/HO_2^{-}$, [4]electron transfer from the stilbenoid anion to $HO_2^{\bullet}$ (red arrow), [5]proton transfer to HO_2^{-}.

4.2. In situ controlled-potential electrolytic ESR analyses of $O_2/O_2^{\bullet-}$ with piceatannol

To confirm the differences in the PCET mechanisms from stilbenoids to $O_2^{\bullet-}$, the CV solutions under an applied potential of −1.3 V corresponding to the electrogeneration of $O_2^{\bullet-}$ (Equation (1)), were analyzed using ESR spectral measurements in an in situ electrolytic cell (Figure S1). The ESR spectrum was obtained only with $PiceH_4$, implying that PCET involving PT and ET from $PiceH_4$ to $O_2^{\bullet-}$ occurred, forming a product radical (Figure 4(a)). Next, the hyperfine coupling constants for hydrogen (a_H/mT) were simulated based on the measured ESR spectra.

Further, spin distributions on the structures of the product radicals ($PiceH_2^{\bullet-}$) were calculated using DFT-(U)B3LYP/PCM/6–311+G(d,p) with NBO analysis (Figure 4(b)). In addition, charges on carbons bonded to hydrogen are indicated. Based on the calculation results, the simulated a_H values were assigned to the hydrogen of $PiceH_2^{\bullet-}$ (H^a–H^h: 0.298, 0.279, 0.176, 0.062, 0.061, 0.058, 0.057, and 0.001 mT).

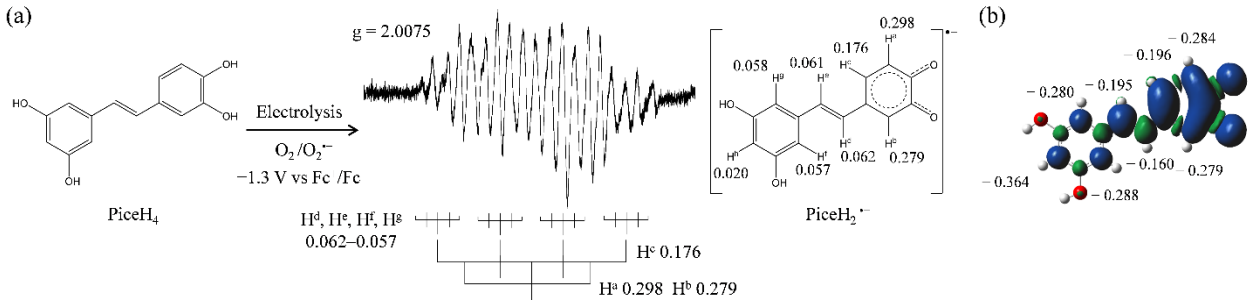

Figure 4. (a) ESR spectra for O_2 (4.8×10^{-3} mol dm^{-3}) in DMF with $PiceH_4$ (1.0×10^{-3} mol dm^{-3}) obtained by the in situ controlled-potential (−1.3 V vs. Fc^+/Fc) electrolysis of solutions containing TPAP (0.1 mol dm^{-3}); radical structures with g-values and appropriate hyperfine coupling constants for hydrogen (a_H/mT) were obtained using simulations based on the measured spectra; (b) spin distribution on $PiceH_2^{\bullet-}$ calculated using DFT-(U)B3LYP/PCM/6–311+G(d,p) with NBO analysis; charges distributed on carbons bonded to hydrogen are indicated.

Interestingly, spins are primarily distributed in the B ring (H^a–H^e) and throughout the molecule of $PiceH_2^{\bullet-}$, as shown in the ESR results. In the CVs shown in Figure 2, a reversible redox couple (pc6/pa6) derived from the product appeared, indicating that the product was a quinoid radical ($PiceH_2^{\bullet-}$) derived from the catechol moiety of the B ring and suggesting that the reaction site of PCET was influenced by the structural differences between $PiceH_4$ and $RsvH_3$. In addition, the a_H values obtained from the ESR spectrum were assigned to the hydrogen on another phenolic ring (A ring, H^f–H^h) and the linked ethylene bridge (stilbene double bond, H^d and H^e), clarifying that the coplanar stilbene moiety contributes to PCET at the catechol moiety. A similar

248 role of the stilbene moiety in contributing the PCET reaction is expected to occur in the $RsvH_3$
249 molecule, although it was suggested that its product radical, generated via PCET, decomposes
250 upon a subsequent reaction (the ESR spectrum was undetectable).

251 Analogous to the CV and ESR results, $RsvH_3$ and $PiceH_4$ scavenge the electrogenerated $O_2^{\bullet-}$
252 via PCET based on their structural characteristics as polyphenol stilbenoids. To the best of our
253 knowledge, this is the first report of the ESR spectrum of the piceatannol radical, which was
254 made observable using the in situ spectroelectrochemical system in well-dried aprotic DMF
255 solution. In addition, a difference in the stabilities of their product radicals ($PiceH_2^{\bullet-}$ and $RsvH^{\bullet-}$)
256 based on the involvement of the catechol moiety implies a difference in the details of the PCET
257 mechanism.

258 4.3. DFT analyses of PCET from $PiceH_4$ to $O_2^{\bullet-}$

259 4.3.1. Optimized structures of $PiceH_4$ and its deprotonated anion

260 To elucidate the mechanism of the PCET between $PiceH_4$ and $O_2^{\bullet-}$ in DMF, DFT calculations
261 were conducted using the B3LYP, M06-2X, and TPSSh hybrid functionals with the PCM
262 method. We focus on the B3LYP results below unless otherwise noted, because the three
263 functionals showed similar results. First, the stable conformations of $PiceH_4$ (Figure S2) and the
264 structures of its anions ($^{a}PiceH_3^-$, $^{b}PiceH_3^-$, $^{c}PiceH_3^-$, and $^{d}PiceH_3^-$) after the initial PT were
265 obtained by energy scanning of the dihedral angle around the four OHs and stilbene moiety
266 (Tables S2 and S3). Figure 5 shows the optimized structures and Gibbs free energy changes
267 ($\Delta G°$/kJ mol^{-1}, 298.15 K) along the initial PT (M06-2X and TPSSh results are shown in Figure
268 S3). Then, charge distribution on the OH protons of $PiceH_4$ obtained using NBO analysis were
269 indicated.

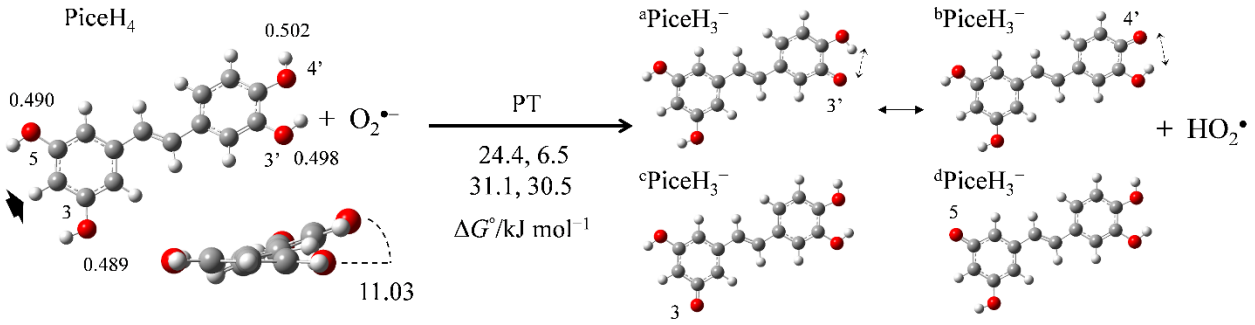

Figure 5. Optimized structures of piceatannol ($PiceH_4$) and deprotonated anions ($^{a}PiceH_3^-$, $^{b}PiceH_3^-$, $^{c}PiceH_3^-$, and $^{d}PiceH_3^-$) along the proton transfer from its hydroxyl group (3OH, 5OH, 3'OH, and 4'OH) to $O_2^{\bullet-}$ in DMF, calculated using the DFT-B3LYP/PCM/6-311+G(d,p); charges distributed on the four OH protons of $PiceH_4$ obtained using NBO analysis and $\Delta G°$s (kJ mol^{-1}, 298.15 K) of proton transfer are indicated.

The optimized structures revealed that the dihedral angle of the two phenolic rings around the stilbene double bond of $PiceH_4$ is 11.03°, and its anion has an approximately planar structure in DMF. Comparing the charges on the four OH protons of $PiceH_4$ (3′OH: 0.498, 4′OH: 0.502, 3OH: 0.489, and 5OH: 0.490), the acid–base reactivities of proton (acidity) slightly higher at 3′OH and 4′OH in the catechol moiety than those at 3OH and 5OH. Similarly, the $\Delta G°$s indicate that the deprotonation at 3′OH and 4′OH forming $^{a}PiceH_3^-$ (24.4) and $^{b}PiceH_3^-$ (6.5) is more plausible than that at 3OH and 5OH forming $^{c}PiceH_3^-$ (31.1) and $^{d}PiceH_3^-$ (30.5), respectively, owing to the intramolecular hydrogen bond at two catechol oxygens (3′OH—H—4′O) in the anions. According to these calculations, PT was initiated at 3′OH or 4′OH, which forms $^{a}PiceH_3^-$ or $^{b}PiceH_3^-$, respectively.

4.3.2. Changes in HOMO–LUMO relation during PCET between $PiceH_4$ and $O_2^{\bullet-}$

The mechanistic analysis of PCET between $O_2^{\bullet-}$ and $PiceH_4$ was conducted using frontier molecular orbital analysis (Figure 6). The HOMO–LUMO (hartree/a.u.) relation changes during

289 the PCET (M06-2X and TPSSh results are shown in Figure S4). Some reactant species, $PiceH_4$,
290 $PiceH_3^-$, $O_2^{\bullet-}$, and $HO_2^{\bullet}$, coexist in the experimental solutions after the initial PT. The HOMO
291 energies of $PiceH_4$ (−0.21001) and its anions ($^aPiceH_3^-$:−0.16988, $^bPiceH_3^-$:−0.16564) were
292 much higher than the SOMO energy of $HO_2^{\bullet}$ (−0.31659), indicating that $HO_2^{\bullet}$ rather than $O_2^{\bullet-}$
293 (−0.15933) was the electron acceptor. Meanwhile, CV revealed that $PiceH_4$ scavenged $O_2^{\bullet-}$ and
294 $HO_2^{\bullet}$ formed after the initial PT (Figure 1a). Therefore, $PiceH_3^-$ was the electron donor as shown
295 in the downhill energy relation (bold red lines). The HOMO–LUMO energies changed during PT
296 from $PiceH_4$ to $O_2^{\bullet-}$, forming $PicesH_3^-$ and $HO_2^{\bullet}$, respectively. Moreover, the HOMO–LUMO
297 relation between the products (i.e., $^aPiceH_3^{\bullet}$/$^bPiceH_3^{\bullet}$ and HO_2^-) upset after the subsequent ET
298 (red dotted lines), suggesting that reverse ET proceed. However, the HOMO (−0.27731) of H_2O_2
299 is lower than that of HO_2^- (−0.16694), indicating that the second PT prevents the reverse ET.
300 Hence, the second PT predominantly determined the direction of ET. This HOMO–LUMO
301 relation is similar whether the second PT occurs from 4'OH forming $^aPiceH_2^{\bullet-}$ (−0.16675) or
302 from 3OH/5OH forming $^bPiceH_2^{\bullet-}$ (−0.18008). As a result of the frontier molecular orbital
303 analysis, the net PCET between $O_2^{\bullet-}$ and $PiceH_4$ involved one ET and two PTs, resulting in the
304 formation of H_2O_2.

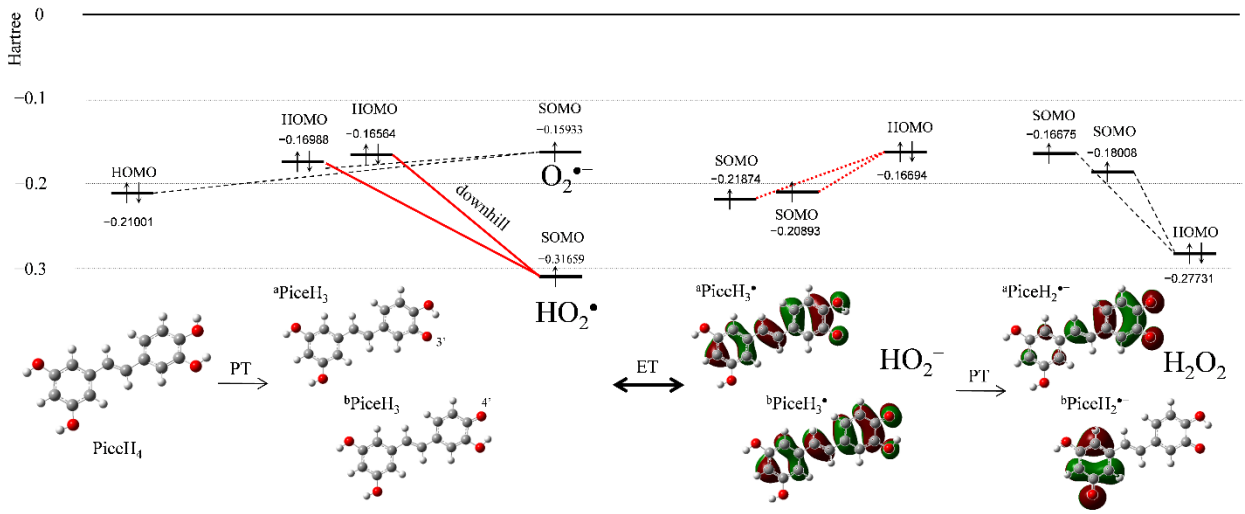

305

306 **Figure 6.** Changes in HOMO−LUMO energies (Hartree/a.u.) during proton-coupled electron
307 transfer between piceatannol ($PiceH_4$) and $O_2^{\bullet-}$ in DMF calculated using DFT-B3LYP/PCM/6-
308 311+G(d,p).

309 4.3.3. Gibbs free energy changes in PCET from $PiceH_4$ to $O_2^{\bullet-}$

310 $\Delta G°$s (kJ mol^{-1}, 298.15 K) along the PCET were calculated using the vibrational frequency
311 calculation combined with the PCM method for the thermodynamically mechanistic analysis of
312 the $O_2^{\bullet-}$ scavenging by $PiceH_4$ in DMF (Table S4). Figure 7 shows the redox equilibrium scheme
313 and the $\Delta G°$s of PCET involving one ET and two PTs from $PiceH_4$ to $O_2^{\bullet-}$, calculated using the
314 B3LYP/PCM/6-311+G(d,p) method (M06-2X and TPSSh results are shown in Figure S5). The
315 $\Delta G°$s of the individual reactions of the components in Figure 7, ET1–ET3 and PT1–PT4, are the
316 main drivers of the sequential pathway. Because ET1 (354.4) was strongly endergonic, PT1
317 (24.4, 6.5) predominantly formed $^{a}PiceH_3^-$/$^{b}PiceH_3^-$ and $HO_2^{\bullet}$. At the bottom of the panels in
318 Figure 7, PT3 (370.2, 388.2) and ET2 (11.7, 13.6) were endogenous; therefore, the sequential
319 pathway was unlikely to proceed. Thus, the only feasible pathway is a concerted PCET involving
320 one ET and two PTs in one-step, where intermediates are not generated. We refer to this pathway
321 as the 2PCET reaction.[24,26,39,40] Notably, 2PCET must occur in a one-kinetic process among an
322 HB complex formed from the catechol moiety of $PiceH_4$ to $O_2^{\bullet-}$.

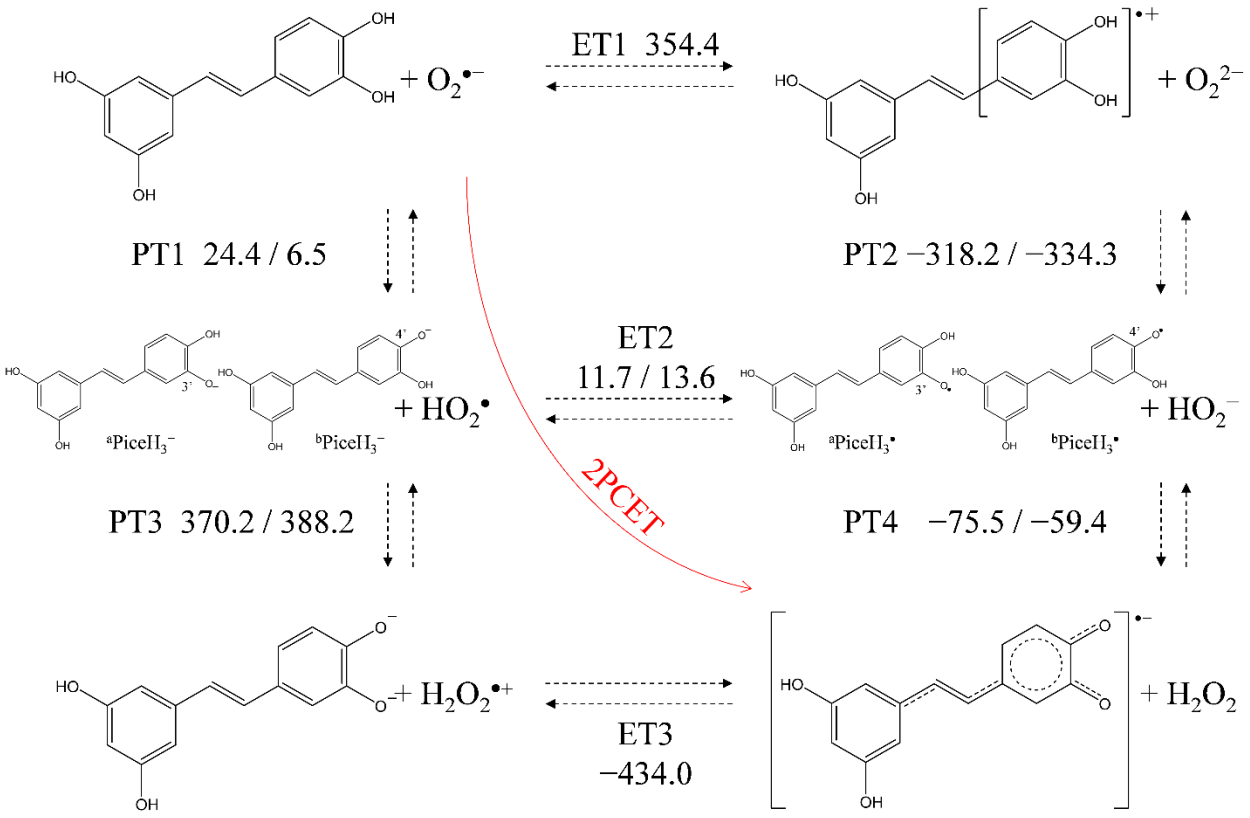

Figure 7. Equilibrium scheme of one electron transfer (ET1–ET3) and two proton transfers (PT1–PT4) from piceatannol ($PiceH_4$) to $O_2^{\bullet-}$ in DMF; $\Delta G°$s (kJ mol^{-1}, 298.15 K) were calculated using DFT-(U)B3LYP/PCM/6-311+G(d,p).

The $\Delta G°$ values of the PCET pathways of $PiceH_4$, $RsvH_3$, and pinosylvin were calculated using B3LYP, M06-2X, and TPSSh functionals for comparison (Table 1). The sum of the $\Delta G°$s of the one ET and two PTs is an energetic driving force of PCET, although that cannot embody it if PCET occurred along a pathway involving an infeasible single PT/ET. Along the plausible sequential pathway based on the electrochemical results (Figure 1), the $\Delta G°$s of PT1 and ET2 for $PiceH_4$ or $RsvH_3$ were endergonic obtained using each functional. Thus, 2PCET was the only feasible pathway for each compound (Table 1). However, the $\Delta G°$s of the total values for pinosylvin (B3LYP: −0.1, M06-2X: 19.1, TPSSh: −2.3) were similar to those for $RsvH_3$ (0.4, 14.0, and −4.9) but larger than those for $PiceH_4$ (−44.8, −31.0, and −34.0, respectively),

inconsistent with the electrochemical results. Thus, the $\Delta G°$ values alone cannot explain the higher reactivities of $PiceH_4$ than those of $RsvH_3$ and pinosylvin toward electrogenerated $O_2^{\bullet-}$ observed in the loss of reversibility (Figure 1).

Table 1. $\Delta G°$ values (kJ mol^{-1}, 298.15 K) of proton-coupled electron transfer from piceatannol ($PiceH_4$), *trans*-resveratrol ($RsvH_3$), pinosylvin, to $O_2^{\bullet-}$ in DMF, calculated using B3LYP, M06-2X, and TPSSh functionals, with the PCM/6-311+G(d,p) basis set

	Stilbenoids	[1]PT1	PT2	PT3	PT4	ET1	ET2	ET3	[2]total
B3LYP	[3]$PiceH_4$	18.9	−318.2	370.2	−75.5	348.9	11.7	−434.0	−44.8
	[3]$RsvH_3$	30.6	−310.4	317.3	−45.8	356.6	15.5	−347.6	0.4
	Pinosylvin	37.3	−314.0	349.5	−66.7	380.6	29.2	−386.9	−0.1
M06-2X	[3]$PiceH_4$	28.3	−347.4	380.6	−96.2	412.6	36.7	−440.0	−31.0
	[3]$RsvH_3$	32.0	−313.8	314.7	−79.3	407.1	61.3	−332.7	14.0
	Pinosylvin	32.3	−341.6	353.0	−75.6	436.4	62.4	−366.3	19.1
TPSSh	[3]$PiceH_4$	11.7	−337.6	369.8	−61.4	365.0	15.6	−415.5	−34.0
	[3]$RsvH_3$	32.0	−289.8	299.9	−76.7	361.5	39.6	−336.9	−4.9
	Pinosylvin	29.9	−313.4	342.4	−75.0	386.2	42.8	−374.6	−2.3

[1]Proton transfer (PT1–PT4) and electron transfer (ET1–ET3). [2]The total values correspond to the sum of those for one ET and two PTs. [3]PT1 and PT2 occur at 3′OH of $PiceH_4$ and 3OH of $RsvH_3$, and PT3 and PT4 occur at 4′OH.

4.3.4. Reaction coordinates and potential energy surfaces of PCET from piceatannol to $O_2^{\bullet-}$

The potential energy surfaces were scanned using the DFT-(U)B3LYP/PCM/6-311+G(d,p) combined with NBO calculations, to gain mechanistic insights into the PCET of $O_2^{\bullet-}/HO_2^{\bullet}$ scavenging by $PiceH_4$. Three elementary steps were assumed during the reaction in DMF: i) formation of a prereactive complex (PRC) via HBs from free reactants, ii) 2PCET via a TS forming a product complex (PC), and iii) PC dissociation yielding the free products. First, we performed structural optimization of feasible PRCs formed with a combination of free reactants, $O_2^{\bullet-}$, $HO_2^{\bullet}$, $PiceH_4$, and $PiceH_3^-$ (step i). Among these, a PRC comprising $PiceH_4$ and $O_2^{\bullet-}$ ($PiceH_4$—$O_2^{\bullet-}$)—formed via the catechol moiety—was more stabilized (71.8 kJ mol^{-1}) by two HBs than the other PRCs. Next, the intermediate complex, PC, and TS, along with the subsequent PCET, were scanned (Supporting Information, Table S5). In addition, some PRCs comprising $PiceH_4$ and $HO_2^{\bullet}$ via single HB at each OH (3OH, 5OH, 3'OH, and 4'OH) were scanned, potentially leading to subsequent reactions. Consequently, only a PRC formed between the catechol moiety of $PiceH_4$ and $O_2^{\bullet-}$ ($PiceH_4$—$O_2^{\bullet-}$) could form a PC ($PiceH_2^{\bullet-}$—H_2O_2) through the 2PCET. And, a TS (step ii) and an intrinsic reaction coordinate (IRC) were found for the 2PCET mechanism, corresponding to moving along the red curve in Figure 7. Figure 8(a) shows the energy profile ($\Delta G°$, kJ mol^{-1}) of the IRC involving the steps (i–iii), where the obtained TS indicates a low activation energy (E_a = 48.6 kJ mol^{-1}) of the 2PCET. Similarly, an energy profile with a TS (E_a = 39.4 kJ mol^{-1}) was obtained using the TPSSh functional (Supporting Information, Figure S6).

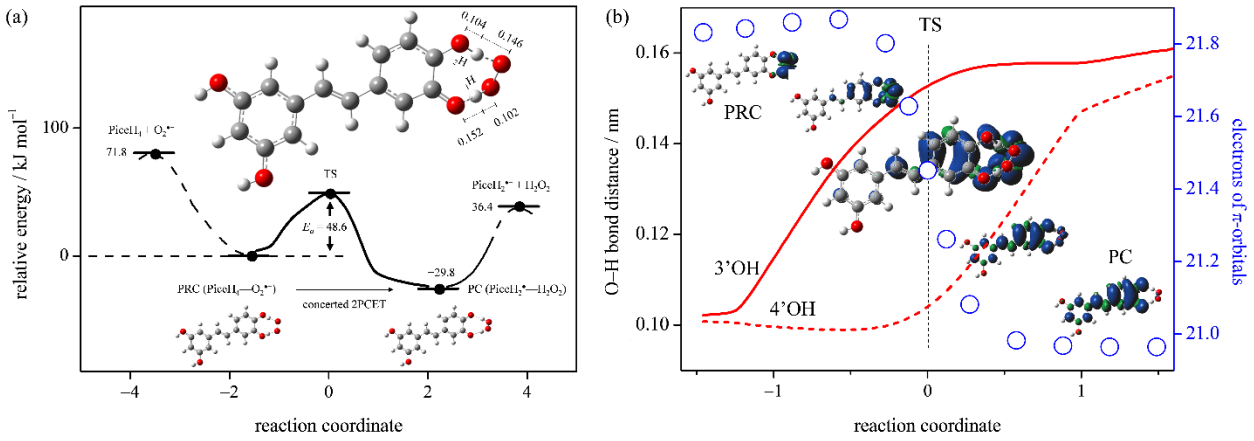

Figure 8. (a) Energy profile (kJ mol^{-1}, 298.15 K) along the reaction coordinate of two-proton-coupled electron transfer from piceatannol ($PiceH_4$) to $O_2^{\bullet-}$ in DMF with the structures of the prereactive complex (PRC, $PiceH_4$–$O_2^{\bullet-}$), transition state (TS), and product complex (PC, $PiceH_2^{\bullet-}$–H_2O_2); (b) changes in the O–H bond distance (3'OH: red bold line, 4'OH: red dotted line, nm) and the number of π-electron of $PiceH_4$ (blue open circles) with the spin distributions; calculations were performed using the DFT-(U)B3LYP/PCM/6-311+G(d,p) with the NBO analyses.

Figure 8(b) demonstrates the relation between the number of electrons in the π-orbital of $PiceH_4$ (blue circles) and the O–H bond distance (3′O–H: red bold line, 4′O–H: red dotted line, nm) along the IRC. The spins were localized on the radicals before and after the TS along the 2PCET, indicating that the radical distributed on $O_2^{\bullet-}$ in the initial PRC was transferred to $PiceH_2^{\bullet-}$ in the PC. The change in the π-electrons of $PiceH_4$ was well correlated with the changes in the spin density distributions on the electron-donor side ($PiceH_4$) and the electron-acceptor side ($O_2^{\bullet-}$). In addition, the TS was electronically characterized by the delocalization of π-electrons over the HB complex (most of the spins were distributed in $O_2^{\bullet-}$–catechol–stilbene double bond moiety). Consequently, the IRC revealed that a 2PCET from $PiceH_4$ (at the catechol moiety) to $O_2^{\bullet-}$ occurred without generating intermediates—such as $HO_2^{\bullet}$—which is a kinetically

superior process in agreement with the electrochemical result. Moreover, the initial PT occurred at 3′OH, forming an intermediate complex ($PiceH_3^-$—$HO_2^\bullet$); further, the second PT occurred at 4′OH (para OH) along the 2PCET without dissociation of the HBs. Herein, we compared Figure 8(a) with the IRC of 2PCET from catechol to $O_2^{\bullet-}$ to elucidate the role of the stilbene moiety of $PiceH_4$. A similar IRC was obtained with a TS for catechol (step ii) using both functionals (Figure S7), where the E_a for $PiceH_4$ (B3LYP: 48.6, TPSSh: 39.4) was lower than that for catechol (52.5, 41.4). Thus, this E_a comparison revealed the kinetically superior $O_2^{\bullet-}$-scavenging ability of $PiceH_4$ compared with that of catechol, implying that the stilbene double bond promotes the 2PCET reaction via the catechol moiety.

These IRC results show that the scavenging of $O_2^{\bullet-}$ by $PiceH_4$ in DMF is governed by 2PCET at the catechol moiety after the formation of PRC between $PiceH_4$ and $O_2^{\bullet-}$. Notably, the coplanar stilbene moiety kinetically promotes 2PCET at the catechol moiety, where the two rings of $PiceH_4$ linked by the double bond of stilbene expand the π-conjugated plane, demonstrating successful scavenging of $O_2^{\bullet-}$.

In conclusion, we investigated the reactivities of piceatannol toward electrogenerated $O_2^{\bullet-}$ in DMF. The primary findings are summarized as follows:

1. Piceatannol scavenges $O_2^{\bullet-}$ via the 2PCET mechanism.
2. 2PCET occurs at the catechol moiety of piceatannol.
3. The stilbene moiety of piceatannol promotes the 2PCET.
4. Piceatannol is better $O_2^{\bullet-}/HO_2^\bullet$ scavenger compared with *trans*-resveratrol and catechol because of its characteristic structure involving both stilbene and catechol moieties.

These findings primarily concern chemical reactions in aprotic DMF solvents. However, our findings may provide mechanistic insights into the scavenging of $O_2^{\bullet-}$ by $PiceH_4$ in biotic structures, such as lipid bilayers, encouraging the use of $PiceH_4$ as a phytoalexin in human health science.

AUTHOR INFORMATION

Corresponding Author

*Tatsushi Nakayama

Department of Pharmacy, Gifu Pharmaceutical University, 1-25-4 Daigaku-nishi, Gifu, 501-1196, Japan; ORCID: 0000-0002-0346-2089; E-mail: tnakayama@gifu-pu.ac.jp; Phone: +81-58-230-8100

Author

Bunji Uno

Current address: Faculty of Pharmacy, Gifu University of Medical Science, 4-3-3 Nijigaoka, Kani, Gifu 509-0923, Japan

Funding

This research was funded by the Iwatani Naoji Foundation, Research Foundation for the Electrotechnology of Chubu, Amano Institute of Technology, and Grant-in-Aid for Scientific Research (grant number 19K16338) from the Japan Society for the Promotion of Science.

Notes

The authors declare no competing financial interest.

ACKNOWLEDGMENT

The authors would like to thank Risa Asahara and Yuki Mori for their experimental assistance.

ABBREVIATIONS USED

ESR, electron spin resonance; DFT, density functional theory; 2PCET, concerted two-proton-coupled electron transfer; ROS, reactive oxygen species; ET, electron transfer; OH, hydroxyl group; SET, single-electron transfer; HAT, hydrogen-atom transfer; PCET, proton-coupled electron transfer; PT, proton transfer; HB, hydrogen bond; GC, glassy carbon; TS, transition state; HOMO, highest occupied molecular orbital; LUMO, lowest unoccupied molecular orbital; PCM, polarized continuum model; NBO, natural bond orbital; CV, cyclic voltammogram; SOMO, singly occupied molecular orbital; PRC, prereactive complex; PC, product complex; IRC, intrinsic reaction coordinate.

ASSOCIATED CONTENT

Supporting Information

CV parameters; in situ controlled-potential electrolytic ESR system; plausible structures of piceatannol; optimized geometries of the compounds; changes in HOMO−LUMO energies; calculated energies and the values; six diabatic electronic states; optimized geometries of the complexes; energy profiles along the reaction coordinates.

Dataset

Tatsushi Nakayama, DFT calculations, concerted two-proton-coupled electron transfer (2PCET) between piceatannol and electrogenerated superoxide in *N*,*N*-dimethylformamide, Mendeley Data, V1, 2024, doi: 10.17632/757frcrxnc.1

REFERENCES

(1) Navarro, G.; Martínez Pinilla, E.; Ortiz, R.; Noé, V.; Ciudad, C. J.; Franco, R. Resveratrol and Related Stilbenoids, Nutraceutical/Dietary Complements with Health-Promoting Actions: Industrial Production, Safety, and the Search for Mode of Action. *Compr Rev Food Sci Food Saf* **2018**, *17* (4), 808–826. https://doi.org/10.1111/1541-4337.12359.

(2) Bhat, K. P. L.; Kosmeder, J. W.; Pezzuto, J. M. Biological Effects of Resveratrol. *Antioxid Redox Signal* **2001**, *3* (6), 1041–1064. https://doi.org/10.1089/152308601317203567.

(3) Münzenberger, B.; Heilemann, J.; Strack, D.; Kottke, I.; Oberwinkler, F. Phenolics of Mycorrhizas and Non-Mycorrhizal Roots of Norway Spruce. *Planta* **1990**, *182* (1), 142–148. https://doi.org/10.1007/BF00239996.

(4) Lee, D.; Cuendet, M.; Schunke Vigo, J.; Graham, J. G.; Cabieses, F.; Fong, H. H. S.; Pezzuto, J. M.; Kinghorn, A. D. A Novel Cyclooxygenase-Inhibitory Stilbenolignan from the Seeds of Aiphanes Aculeata. *Org Lett* **2001**, *3* (14), 2169–2171. https://doi.org/10.1021/ol015985j.

(5) Yao, C. S.; Lin, M.; Liu, X.; Wang, Y. H. Stilbene Derivatives from Gnetum Cleistostachyum. *J Asian Nat Prod Res* **2005**, *7* (2), 131–137. https://doi.org/10.1080/10286020310001625102.

(6) Geahlen, R. L.; McLaughlin, J. L. Piceatannol (3,4,3′,5′-Tetrahydroxy-Trans-Stilbene) Is a Naturally Occurring Protein-Tyrosine Kinase Inhibitor. *Biochem Biophys Res Commun* **1989**, *165* (1), 241–245. https://doi.org/10.1016/0006-291X(89)91060-7.

(7) Hosoda, R.; Hamada, H.; Uesugi, D.; Iwahara, N.; Nojima, I.; Horio, Y.; Kuno, A. Different Antioxidative and Antiapoptotic Effects of Piceatannol and Resveratrol. *Journal of Pharmacology and Experimental Therapeutics* **2021**, *376* (3), 385–396. https://doi.org/10.1124/jpet.120.000096.

(8) Yang, W.; Wang, Y.; Hao, Y.; Wang, Z.; Liu, J.; Wang, J. Piceatannol Alleviate ROS-Mediated PC-12 Cells Damage and Mitochondrial Dysfunction through SIRT3/FOXO3a Signaling Pathway. *J Food Biochem* **2022**, *46* (3), e13820. https://doi.org/10.1111/jfbc.13820.

(9) Cordova-Gomez, M.; Galano, A.; Alvarez-Idaboy, J. R. Piceatannol, a Better Peroxyl Radical Scavenger than Resveratrol. *RSC Adv* **2013**, *3* (43), 20209–20218. https://doi.org/10.1039/c3ra42923g.

(10) Caruso, F.; Tanski, J.; Villegas-Estrada, A.; Rossi, M. Structural Basis for Antioxidant Activity of Trans-Resveratrol: Ab Initio Calculations and Crystal and Molecular Structure. *J Agric Food Chem* **2004**, *52* (24), 7279–7285. https://doi.org/10.1021/jf048794e.

(11) Gülçin, I. Antioxidant Properties of Resveratrol: A Structure–Activity Insight. *Innovative Food Science & Emerging Technologies* **2010**, *11* (1), 210–218. https://doi.org/10.1016/J.IFSET.2009.07.002.

(12) Qiu, J. M.; Qin, C. F.; Wu, S. G.; Ji, T. Y.; Tang, G. T.; Lei, X. Y.; Cao, X.; Xie, Z. Z. A Novel Salvianolic Acid A Analog with Resveratrol Structure and Its Antioxidant Activities in Vitro and in Vivo. *Drug Dev Res* **2021**, *82* (1), 108–114. https://doi.org/10.1002/ddr.21734.

(13) Iuga, C.; Raúl Alvarez-Idaboy, J.; Russo, N. Antioxidant Activity of Trans-Resveratrol toward Hydroxyl and Hydroperoxyl Radicals: A Quantum Chemical and Computational Kinetics Study. *J Org Chem* **2012**, *77* (8), 3868–3877. https://doi.org/10.1021/jo3002134.

(14) Storniolo, C. E.; Moreno, J. J. Resveratrol Analogs with Antioxidant Activity Inhibit Intestinal Epithelial Cancer Caco-2 Cell Growth by Modulating Arachidonic Acid Cascade. *J Agric Food Chem* **2019**, *67* (3), 819–828. https://doi.org/10.1021/acs.jafc.8b05982.

(15) Nanni, E. J.; Birge, R. R.; Hubbard, L. M.; Morrison, M. M.; Sawyer, D. T. Oxidation and Dismutation of Superoxide Ion Solutions to Molecular Oxygen. Singlet vs. Triplet State. *Inorg Chem* **1981**, *20* (3), 737–741. https://doi.org/10.1021/ic50217a019.

(16) Nanni, E. J.; Stallings, M. D.; Sawyer, D. T. Does Superoxide Ion Oxidize Catechol, α-Tocopherol, and Ascorbic Acid by Direct Electron Transfer? *J Am Chem Soc* **1980**, *102* (13), 4481–4485. https://doi.org/10.1021/ja00533a029.

(17) Song, C.; Zhang, J. Electrocatalytic Oxygen Reduction Reaction. In *PEM Fuel Cell Electrocatalysts and Catalyst Layers*; Springer: London, 2008; pp 89–134. https://doi.org/10.1007/978-1-84800-936-3_2.

(18) Biela, M.; Rimarčík, J.; Senajová, E.; Kleinová, A.; Klein, E. Antioxidant Action of Deprotonated Flavonoids: Thermodynamics of Sequential Proton-Loss Electron-Transfer. *Phytochemistry* **2020**, *180*, 112528. https://doi.org/10.1016/j.phytochem.2020.112528.

(19) Singh, P. S.; Evans, D. H. Study of the Electrochemical Reduction of Dioxygen in Acetonitrile in the Presence of Weak Acids. *Journal of Physical Chemistry B* **2006**, *110*, 637–644. https://doi.org/10.1021/jp055296f.

(20) Nakayama, T.; Uno, B. Importance of Proton-Coupled Electron Transfer from Natural Phenolic Compounds in Superoxide Scavenging. *Chem Pharm Bull (Tokyo)* **2015**, *63* (12), 967–973. https://doi.org/10.1248/cpb.c15-00447.

(21) Weinberg, D. R.; Gagliardi, C. J.; Hull, J. F.; Murphy, C. F.; Kent, C. A.; Westlake, B. C.; Paul, A.; Ess, D. H.; McCafferty, D. G.; Meyer, T. J. Proton-Coupled Electron Transfer. *Chem Rev* **2012**, *112* (7), 4016–4093. https://doi.org/10.1021/cr200177j.

(22) Tyburski, R.; Liu, T.; Glover, S. D.; Hammarström, L. Proton-Coupled Electron Transfer Guidelines, Fair and Square. *J Am Chem Soc* **2021**, *143* (2), 560–576. https://doi.org/10.1021/jacs.0c09106.

(23) Nakayama, T.; Uno, B. Reactivities of Hydroxycinnamic Acid Derivatives Involving Caffeic Acid toward Electrogenerated Superoxide in *N*,*N*-Dimethylformamide. *Electrochem* **2022**, *3* (3), 347–360. https://doi.org/10.3390/electrochem3030024.

(24) Nakayama, T.; Uno, B. Concerted Two-Proton-Coupled Electron Transfer from Catechols to Superoxide via Hydrogen Bonds. *Electrochim Acta* **2016**, *208*, 304–309. https://doi.org/10.1016/j.electacta.2016.05.034.

(25) Nakayama, T.; Uno, B. Quinone-Hydroquinone π-Conjugated Redox Reaction Involving Proton-Coupled Electron Transfer Plays an Important Role in Scavenging Superoxide by Polyphenolic Antioxidants. *Chem Lett* **2010**, *39* (3), 162–164. https://doi.org/10.1246/cl.2010.162.

(26) Nakayama, T.; Uno, B. Reactivities of 1,2-, 1,3-, and 1,4-Dihydroxynaphthalenes toward Electrogenerated Superoxide in *N*,*N*-Dimethylformamide through Proton-Coupled Electron Transfer. *Electrochim Acta* **2022**, *436*, 141467. https://doi.org/10.1016/J.ELECTACTA.2022.141467.

(27) Nakayama, T.; Honda, R.; Kuwata, K.; Usui, S.; Uno, B. Electrochemical and Mechanistic Study of Reactivities of α-, β-, γ-, and δ-Tocopherol toward Electrogenerated Superoxide in *N*,*N*-Dimethylformamide through Proton-Coupled Electron Transfer. *Antioxidants* **2022**, *11* (1), 115–128. https://doi.org/10.3390/antiox11010009.

(28) Nakayama, T.; Honda, R. Electrochemical and Mechanistic Study of Superoxide Elimination by Mesalazine through Proton-Coupled Electron Transfer. *Pharmaceuticals* **2021**, *14* (2), 120. https://doi.org/10.3390/ph14020120.

(29) Nakayama, T.; Uno, B. Reactivity of Trans-Resveratrol toward Electrogenerated Superoxide in N,N-Dimethylformamide. *J Agric Food Chem* **2023**, *71* (10), 4382–4393. https://doi.org/10.1021/acs.jafc.2c08105.

(30) Leonard, S. S.; Xia, C.; Jiang, B. H.; Stinefelt, B.; Klandorf, H.; Harris, G. K.; Shi, X. Resveratrol Scavenges Reactive Oxygen Species and Effects Radical-Induced Cellular Responses. *Biochem Biophys Res Commun* **2003**, *309* (4), 1017–1026. https://doi.org/10.1016/j.bbrc.2003.08.105.

(31) Li, D.-D.; Han, R.-M.; Liang, R.; Chen, C.-H.; Lai, W.; Zhang, J.-P.; H. Skibsted, L. Hydroxyl Radical Reaction with Trans-Resveratrol: Initial Carbon Radical Adduct Formation Followed by Rearrangement to Phenoxyl Radical. *J Phys Chem B* **2012**, *116* (24), 7154–7161. https://doi.org/10.1021/jp3033337.

(32) Shang, Y.-J.; Qian, Y.-P.; Liu, X.-D.; Dai, F.; Shang, X.-L.; Jia, W.-Q.; Liu, Q.; Fang, J.-G.; Zhou, B. Radical-Scavenging Activity and Mechanism of Resveratrol-Oriented Analogues: Influence of the Solvent, Radical, and Substitution. *J Org Chem* **2009**, *74* (14), 5025–5031. https://doi.org/10.1021/jo9007095.

(33) Okumura, N.; Uno, B. Electronic Spectra of the Electrogenerated 1,4-Benzoquinone π-Dianion and the Strongly Hydrogen-Bonded Charge-Transfer Complex with Methanol. *Bull Chem Soc Jpn* **1999**, *72* (6), 1213–1217. https://doi.org/10.1246/bcsj.72.1213.

(34) Zhao, Y.; Truhlar, D. G. The M06 Suite of Density Functionals for Main Group Thermochemistry, Thermochemical Kinetics, Noncovalent Interactions, Excited States, and Transition Elements: Two New Functionals and Systematic Testing of Four M06-

Class Functionals and 12 Other Function. *Theor Chem Acc* **2008**, *120* (1–3), 215–241. https://doi.org/10.1007/s00214-007-0310-x.

(35) Jensen, K. P. Bioinorganic Chemistry Modeled with the TPSSh Density Functional. *Inorg Chem* **2008**, *47* (22), 10357–10365. https://doi.org/10.1021/ic800841t.

(36) Perdew, J. P.; Tao, J.; Staroverov, V. N.; Scuseria, G. E. Meta-Generalized Gradient Approximation: Explanation of a Realistic Nonempirical Density Functional. *Journal of Chemical Physics* **2004**, *120* (15), 6898–6911. https://doi.org/10.1063/1.1665298.

(37) Frisch M. J.; Trucks G. W.; Schlegel, H. B.; Scuseria, G. E.; Robb, M. A.; Cheeseman, J. R.; Scalmani, G.; Barone, V.; Petersson, G. A.; Nakatsuji, H.; Li, X.; Caricato, M.; Marenich, A. V.; Bloino, J.; Janesko, B. G.; Gomperts, R.; Mennucci, B.; Hratchian, H. P.; Ortiz, J. V.; Izmaylov, A. F.; Sonnenberg, J. L.; Williams-Young, D.; Ding, F.; Lipparini, F.; Egidi, F.; Goings, J.; Peng, B.; Petrone, A.; Henderson, T.; Ranasinghe, D.; Zakrzewski, V. G.; Gao, J.; Rega, N.; Zheng, G.; Liang, W.; Hada, M.; Ehara, M.; Toyota, K.; Fukuda, R.; Hasegawa, J.; Ishida, M.; Nakajima, T.; Honda, Y.; Kitao, O.; Nakai, H.; Vreven, T.; Throssell, K.; Montgomery Jr., J. A.; Peralta, J. E.; Ogliaro, F.; Bearpark, M. J.; Heyd, J. J.; Brothers, E. N.; Kudin, K. N.; Staroverov, V. N.; Keith, T. A.; Kobayashi, R.; Normand, J.; Raghavachari, K.; Rendell, A. P.; Burant, J. C.; Iyengar, S. S.; Tomasi, J.; Cossi, M.; Millam, J. M.; Klene, M.; Adamo, C.; Cammi, R.; Ochterski, J. W.; Martin, R. L.; Morokuma, K.; Farkas, O.; Foresman, J. B.; Fox, D. J. *Gaussian 16, Rev. B.01*; Gaussian, Inc.: Wallingford, CT, USA, 2016.

(38) Reed, A. E.; Weinstock, R. B.; Weinhold, F. Natural Population Analysis. *J Chem Phys* **1985**, *83* (2), 735–746. https://doi.org/10.1063/1.449486.

(39) Quintero-Saumeth, J.; Rincón, D. A.; Doerr, M.; Daza, M. C. Concerted Double Proton-Transfer Electron-Transfer between Catechol and Superoxide Radical Anion. *Physical Chemistry Chemical Physics* **2017**, *19* (38), 26179–26190. https://doi.org/10.1039/c7cp03930a.

(40) Nakayama, T.; Honda, R.; Kuwata, K.; Usui, S.; Uno, B. Electrochemical and Mechanistic Study of Superoxide Scavenging by Pyrogallol in *N*,*N*-Dimethylformamide through Proton-Coupled Electron Transfer. *Electrochem* **2022**, *3* (1), 115–128. https://doi.org/10.3390/electrochem3010008.

592 TOC

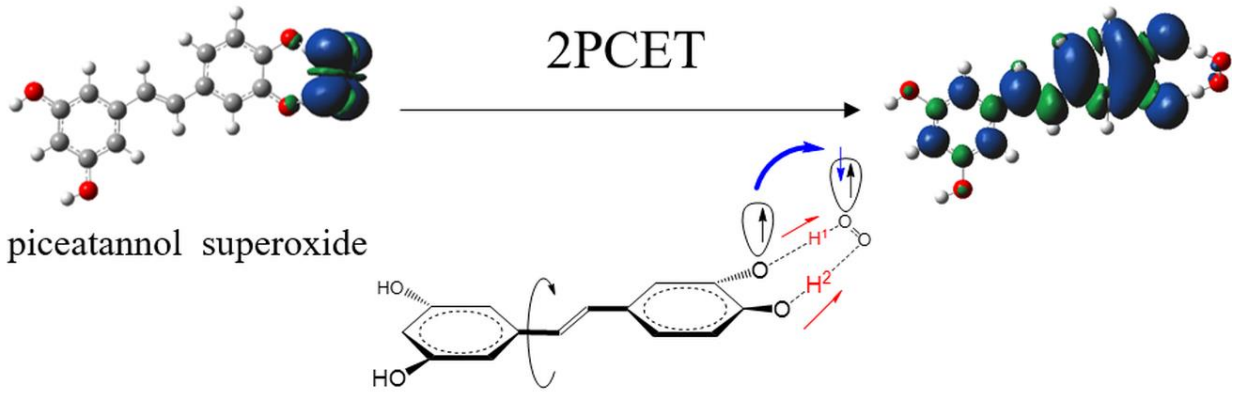

593